Towards a Conceptual Model of a Bio-Robotic AUV: Pectoral Fin Hydrodynamics

Rajat Mittal, Imran Akhtar & Meliha Bozkurttas
Department of Mechanical and Aerospace Engineering
The George Washington University
Washington DC 20052
Email: mittal@gwu.edu

Fady. M. Najjar
Center for Simulation of Advanced Rockets
University of Illinois at Urbana-Champaign
Urbana, IL 61801
Email: f-najjar@uiuc.edu

***Abstract*— Numerical simulations have been used to examine the performance of flapping foils. It is envisioned that these flapping foils will be employed as pectoral fins in a bio-robotic AUV (BAUV) and a detailed parametrization of the hydrodynamic performance of these foils will allow for the development of a high-fidelity dynamical model of the BAUV. In the long term, it is expected that this dynamical model will provide a rational basis for the design, sizing and placement of these fins. In the current paper, we describe a sequence of simulations that explore the effect of pitch-bias angle on the hydrodynamic performance of a 2D flapping foils. In another sequence of simulations, we have examined the effect of foil aspect ratio on its performance and results relating to this study are also included.**

I. Introduction

There is currently an ongoing effort to develop a bio-robotic AUV (BAUV) that can match the underwater search capabilities of marine mammals systems (MMS), specifically dolphins. The key technological advances required in order to reach this goal are:

1) An engineered sonar system that matches the performance of MMS.
2) An AUV platform that can match the maneuvering performance of MMS, thereby allowing it to avoid mines and other obstacles during the search process.

The ONR/DARPA Biosonar Program is directed towards tackling the first of these technological problems whereas the FY03 ONR MURI program (*Integrated Artificial Muscle, High-Lift Bio-Hydrodynamics and Neuro-Control for Biorobotic Autonomous Undersea Vehicles*) will address the second aspect. The specific goal of the MURI program is to develop an artificial-muscle based biomimetic pectoral fin which, when attached to an AUV platform will confer significant improvements in its maneuverability. A conceptual simulation of the BAUV which incorporates appropriate models for the biosonar as well as the vehicle dynamics and control would prove to be a significant asset in guiding the preliminary design of this BAUV. Development and testing of such a conceptual model forms the main goal of the current project. The project has two near-term objectives: (a) Parametrization and analysis of hydrodynamic forces generated by flapping pectoral fins which is being carried out by the George Washington University team and (b) development and testing of a dynamical model of the BAUV which is being spearheaded by S. Singh at University of Nevada at Las Vegas. Work being carried under the first component is presented here whereas the second component will be described in the companion paper by S. Singh.

II. BAUV Configuration and Modelling Approach

It is assumed that the BAUV being modeled has multiple (> 2) pectoral fins that are arranged symmetrically around the body of the AUV [1]. Figure 1 shows a schematic of a typical AUV with one pair of pectoral fins. Each fin is assumed to execute a combined pitch-and-heave motion which is given by

$$z = z_1 \sin(2\pi f t) \tag{1}$$

$$\alpha = \alpha_0 + \alpha_1 \cos(2\pi f t) \tag{2}$$

where z_1 is the heave amplitude, f the flapping frequency, and α_0 and α_1 are the mean (bias) pitch angle and pitch amplitude, respectively. It is further assumed that the fins flap with a fixed frequency and amplitude and the primary control parameters are the pitch bias (α_0) and amplitude (α_1)of the fin. As a result of this motion, the fin experiences a time varying hydrodynamic force (which can be resolved into a thrust component F^x and a lift component F^z) and a pitching moment M^y. These components can be approximated as sinusoidal functions of the form

$$F^x = F^x_0 + F^x_1 e^{i2\pi f t} + F^x_2 e^{i4\pi f t} \tag{3}$$

$$F^z = F^z_0 + F^z_1 e^{i2\pi f t} + F^z_2 e^{i4\pi f t} \tag{4}$$

$$M^y = M^y_0 + M^y_1 e^{i2\pi f t} + M^y_2 e^{i4\pi f t} \tag{5}$$

The hydrodynamic forces on the pectoral fin also produce rolling (M^x), and yawing (M^z) moments on the BAUV which affect the dynamics of the BAUV. The following are the key non-dimensional parameters that govern the performance of a rigid, rectangular, flapping foil: Re, St, α_0, α_1, z_1/c and s/c where $Re = cU_\infty/\nu$, $St = 2z_1 f/U_\infty$, c the foil chord and s the foil span. In some previous studies, a quasi-steady assumption has been employed in order to relate the hydrodynamic forces to the foil parameters. For instance the lift on a pitching-heaving foils has been estimated as:

$$F^z(t) = \rho U^2_\infty c_{l_\alpha}[\alpha + \dot{z}/U_\infty + K(\dot{\alpha}/U_\infty)] \tag{6}$$

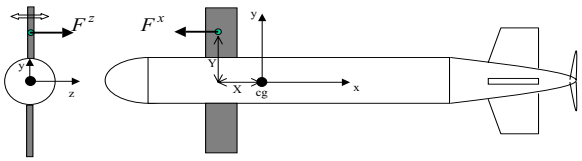

Fig. 1. Schematic of a BAUV with one pair of pectoral fins

where c_{l_α} is the lift coefficient per unit angle-of-attack and K is a known constant. The above parametrization assumes that the instantaneous lift force generated by a flapping foil is equal to that produced by a static airfoil at an equivalent angle-of-attack. This is likely a reasonable approximation for low amplitude wing-flutter where such approximations have been employed in the past. However, it is well known [2], [3] that unsteady mechanisms dominate the flow over flapping foils undergoing large amplitude motions and quasi-steady estimates can be significantly erroneous. In the current effort we therefore plan a first of its kind study where numerical simulations will be used to create a comprehensive performance map of 2D and 3D flapping foil.

In order to understand the scope of this problem, consider that the force coefficients are function of all the major non-dimensional parameters:

$$F_i^x; F_i^z; M_i^y = fn(\alpha_0, \alpha_1, Re, St, z_1/c, s/c); i = 0, 1, 2 \quad (7)$$

It is assumed that the BAUV pectoral fins operate at a fixed, z_1/c and s/c and the primary control inputs are the foil pitch parameters (α_0, α_1). However since the velocity of the BAUV is allowed to vary, this will produce variations in both the Reynolds and Strouhal numbers and therefore, the effect of these parameters on the performance also has to be parameterized. Thus in order to adequately parameterize the performance of the flapping foil for the BAUV conceptual model, the CFD simulations need to extract the dependence of the force coefficients on the four parameters α_0, α_1, Re and St. In addition, selection of an appropriate planform for the foil requires an understanding of the effect of the foil aspect-ratio on the foil performance and this is another goal of the current study. Finally, from a fundamental point-of-view, it would be useful to analyze the wake dynamics for low aspect-ratio foils viz-a-viz what is known regarding 2D flapping foils [4] [5] [6].

III. Numerical Method

The numerical method employed for this study has to be capable of simulating flow past two- and three-dimensional moving bodies. Furthermore, the method should be time-accurate and be able to accurately predict the evolution of the vorticity field. Finally, the method should be computationally efficient so as to allow us to span a large parameter space. The conventional approach to such simulations is to discretize the governing equations on a structured or unstructured mesh that conforms to the body. In this approach, the mesh is modified at every time step so as to conform to the moving body. Although this approach has been used quite extensively for a variety of problems [7] [18] there are some disadvantages inherent to it. In particular, remeshing can introduce significant complexity into the algorithm and can have a negative impact on the accuracy, robustness and efficiency of the solver.

An alternative to the above approach is the so called Cartesian grid method [9] [10]. The distinguishing feature of this method is that the governing equations are discretized on a Cartesian grid which does not conform to the immersed boundary. This greatly simplifies grid generation and also retains the relative simplicity of the governing equations in Cartesian coordinates. Therefore, this method has distinct advantages over the conventional body-fitted approach in simulating flows with moving boundaries and/or complicated shapes. The framework of this method can be considered Eulerian-Lagrangian, wherein the immersed boundaries are explicitly tracked as surfaces in a Lagrangian fashion, while the flow computations are performed on a fixed Eulerian mesh. This approach affords the advantage of pure Lagrangian methods such as explicit interface information, without the ambiguities associated with *a-posteriori* reconstruction of the interface from an advected scalar (such as in Volume-of-Fluid, level-set or phase-field methods). Furthermore, remeshing is eliminated and this circumvents many of the difficulties associated with mesh management. In contrast to purely Eulerian interface capturing approaches (diffuse interface methods) the current method also treats the immersed boundaries as sharp interfaces.

In our previous papers [9] [10] we have described the development of a finite-volume based Cartesian grid method for two-dimensional incompressible flow problems. This method was shown to be very flexible in handling a wide variety of moving boundary problems [11] [12]. Furthermore, extensive validation and testing demonstrated the relatively high accuracy and robustness of the numerical method [9] [10]. This method however, relied on the use of "cut-cells" and the extension of this cut-cell approach to three-dimensions was found to be quite difficult.

A new finite-difference based Cartesian grid method has therefore been developed which does not rely on the cut-cell approach. The method is therefore easily extended to three-dimensions. The method employs a second-order central difference scheme in space and a second-order accurate fractional-step method for time advancement. The Eulerian form of the Navier-Stokes equations are discretized on a Cartesian mesh and boundary conditions on the immersed boundary are imposed through a "ghost-cell" procedure. In this procedure, we identify cells that are just inside the immersed boundary. The discrete equations for these cells are then formulated so as to satisfy the boundary condition on the nearby boundary to second-order accuracy. These equations are then solved in a fully-coupled manner with the governing flow equations of all the other regular fluid cells. Care is also taken to ensure that these equations satisfy both local as well as global mass conservation constraints as well as pressure-velocity compatibility relations.

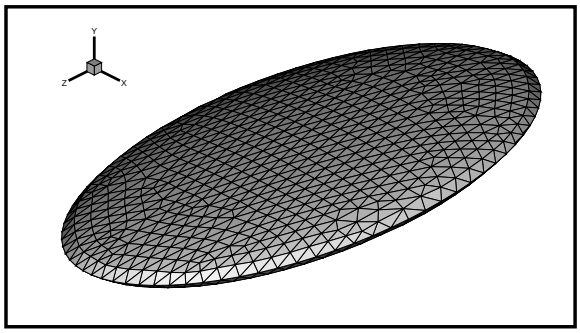

Fig. 2. An elliptical disk defined in terms of a triangulated mesh.

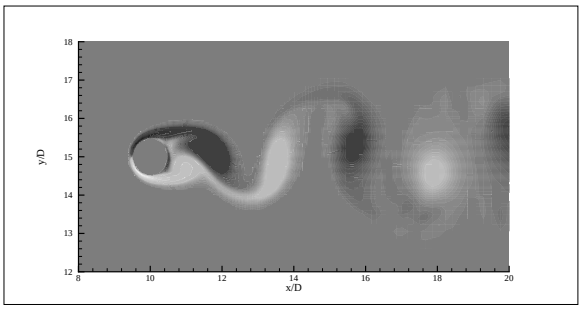

Fig. 3. Spanwise vorticity contour plots for flow past a circular cylinder at $Re_d = 200$.

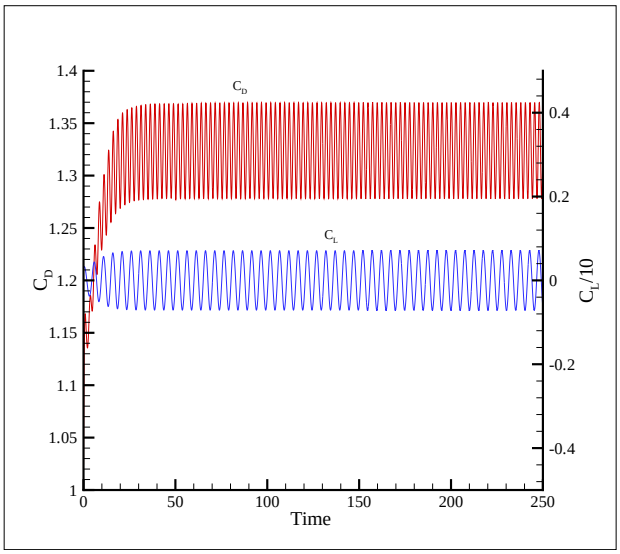

Fig. 4. Temporal variation of drag and lift coefficient of circular cylinder at $Re_d = 200$.

The geometry of the immersed boundary itself can be defined in a number of different ways. In order to provide maximum compatibility with existing CAD programs and commercial CFD packages, we have incorporated in this code, the ability to accept immersed boundaries defined in terms of an unstructured triangular mesh. Figure 2 show the unstructured surface description of an ellipical foil, results for which will be shown in a later section of this paper.

IV. Results

In this section, we present some preliminary results obtained from this newly developed code. These include initial validation studies as well as demonstration of the capability of the code for conducting flapping foil simulations.

A. Validation

Initial validation studies have focussed on simulating canonical flows including backward-facing step flow, flow past a circular and flow past a sphere, and comparing simulations results against established experimental and computational data. Here we present some limited results for flow past a circular cylinder.

For this study we have chosen a low Reynolds numbers ($Re = U_\infty D/\nu$ where U_∞ is the free-stream velocity D is the cylinder diameter and ν is the kinematic viscosity of the fluid) of Re=100 and 200. The computations have been carried out on a $30D \times 30D$ computational domain with the cylinder center located at $(10D, 15D)$. At the inflow $(x = 0)$, the lower $(y/D = 0)$ and upper $(y/D = 30)$ boundaries, a uniform free-stream velocity is imposed, while a convective boundary condition is applied at the outflow $(x/D = 30)$ boundary. The computational grid consists of 240×120 cells and the time step size, $\Delta t U_\infty/D$, is set to 5×10^{-3}. The computations have been integrated temporally for over 20 shedding cycles and results analyzed subsequent to the flow reaching a stationary state.

Figure 3 presents contours of the instantaneous spanwise vorticity for the flow past a circular cylinder at Re=200. The classical Karman shedding mechanism is well captured. Figure 4 illustrates the temporal variations of the instantaneous lift and drag coefficients. Both coefficient exhibits a dominant periodic oscillation associated with the Karman vortex shedding process. The current computations predict a Strouhal number of 0.20 which matches well with the value of 0.198 measured by Williamson [13]. The mean drag coefficient is computed to be 1.33 and this also agrees reasonably well with previous published values of 1.35 [9] and 1.38 [14], respectively.

B. Flapping Foils

1) 2D Flapping Foil with Pitch Bias: A set of 2D simulations have been carried out to examine the effect of pitch-bias angle on the performance of flapping foils. For this initial study we have chosen a 20% thick elliptic airfoil at a Reynolds number of 300. The heave amplitude (z_1/c), Strouhal number and pitch amplitude (α_1) are fixed at values of 0.5, 0.7 and 40^o respectively and we examine the flow and foil performance for pitch-bias angles (α_0) of 0^o, 10^o, 20^o and 30^o.

Figure 5 shows spanwise contour plots for the four different pitch-bias cases at a phase when the foil is at its center position and moving upwards. For the zero pitch-bias case, a vortex street made up of equal strength clockwise and counter-clockwise vortices is observed. Furthermore, as expected this

street is oriented along the streamwise direction. However for pitch-bias angles of 10^o and 20^o we observed a different wake topology. In these wakes, we observe that each cycle produces a strong vortex dipole which convects into the fourth-quadrant (4 O'Clock direction) as well as a small counterclockwise vortex that convects along the streamwise direction. For the highest pitch-bias case of 30^o there is a further modification in the wake topology wherein the small clockwise vortex also gets entrained by the vectored propulsive jet and convect in the direction of the dipole. Furthermore, for this case we also observe the formation of a strong leading-edge stall vortex due to the large incidence angle of the flow.

Change in the pitch-bias angle has a significant effect on the hydrodynamic forces produced by the flapping foil. Figure 6 shows the variation of the mean thrust and lift coefficients with the pitch-bias angle. It can be seen that for a bias-angle greater than about 15^o, the foil produces negative thrust or drag. This is inline with the recent experiments of Triantafyllou et al. [15] for a rolling-pitching foil. Furthermore, the mean lift coefficient increases almost linearly from zero to about one as the pitch-bias angle is increased to 30^o. This rapid increase in mean lift with pitch-bias angle suggests that the pitch-bias would be an effective control parameter for producing pitch-up force and rolling moment for rapid and precise maneuvering.

2) Comparison of 2D and 3D Flapping Foils: The objective of this set of simulations is to examine the effect of foil aspect-ratio $\left(AR = \text{span}^2/\text{area}\right)$ on the foil performance as well as the vortex topology of the wake. Fish pectoral fins tends to be of low aspect-ratio with typical values in the vicinity of about 2.0 [16] [17] and it is expected that the BAUV pectoral fin will also be of a similar aspect-ratio. Despite this preponderance of low aspect-ratio fins in the nature, most of the theoretical, computational and experimental work has been carried out for infinite span (2D) foils. Some recent studies [3] [15] [18] [19], have examined the performance of realistic low aspect-ratio foils but it is fair to say that no systematic effort has yet been made to examine the effect of aspect-ratio on the foils performance. Such knowledge would obviously be crucial in designing/sizing a biomimetic pectoral fin. Furthermore, from a fundamental point-of-view, it is of interest to examine the vortex dynamics and wake topology associated with low-aspect ratio flapping foils viz-a-viz corresponding infinite aspect-ratio foils. To this end, we have initiated a set of simulations of flapping foils of a range of aspect-ratios and some preliminary results from these computations are presented here.

For these simulations we employ foils which are ellipsoidal in shape (see Fig. 2) wherein the geometry of the foil is specified in terms of the three major-axes (a_x, a_y, a_z) where a_x, a_y and a_z are also the foil chord (c), thickness and span (s) respectively. Note that the aspect ratio of these foils is given by $AR = \frac{4}{\pi}(a_z/a_x)$ Three different ellipsoidal foils have been examined: A two-dimensional ($AR = \infty$) foil with major-axes $(1.0, 0.2, \infty)$; a circular planform foil with major-axes $(1.0, 0.2, 1.0)$ and $AR = 1.27$ and finally, an elliptical planform foil with major-axes $(1.0, 0.2, 2.0)$ and $AR = 2.55$.

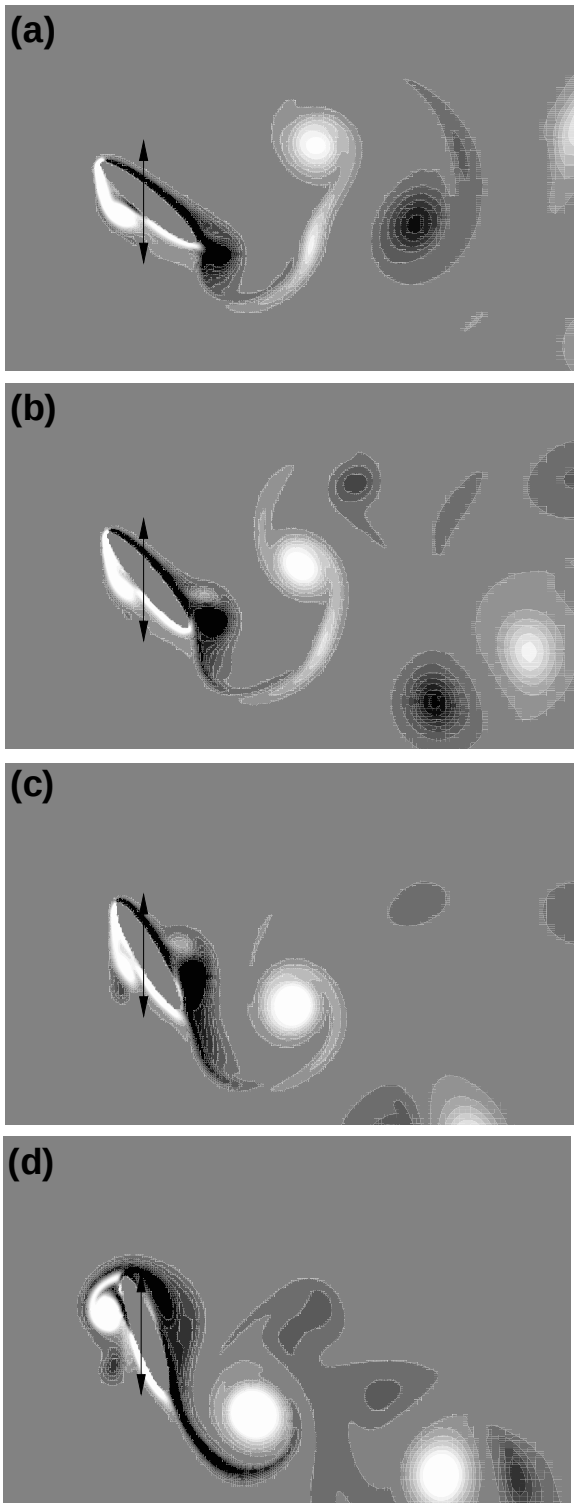

Fig. 5. Spanwise vorticity contour plots for a 2D heaving foil with four different pitch-bias angles. (a) $\alpha_0 = 0$ (b) 10^o (c) 20^o (d) 30^o. The arrow indicates the extent of motion of the foil centroid.

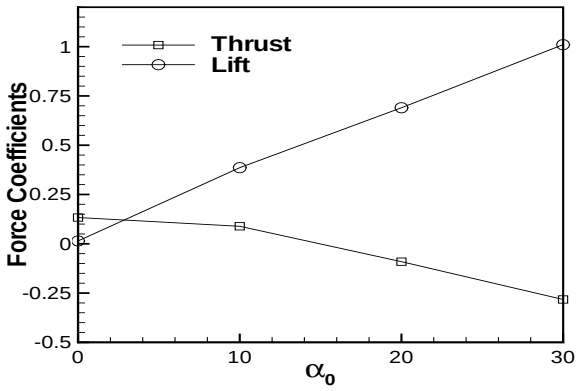

Fig. 6. Effect of pitch-bias angle on the mean thrust and lift coefficient of the flapping foil.

A low Reynolds number of 100 is chosen for these simulations and the Strouhal number is fixed at a value of 0.5. Furthermore, for these simulations the flapping parameters are fixed at $z_1/c = 0.25$ and $\alpha_0 = \alpha_1 = 0$. Thus in these first set of simulations, we focus on a purely heaving motion with no pitch variation.

Figure 7 shows a sequence of spanwise vorticity contour plots for the 2D foil at four phases in its flapping motion. As expected, it is observed that the motion results in the formation of large spanwise vortices which convect into the foil wake. These vortices arrange themselves in a somewhat regular pattern in the near wake which resembles the inverse Karman vortex street observed by others [4], [5] for 2D flapping foils.

In Figure 8(a) is plotted one isosurface of enstrophy for the case of the circular disk whereas Figure 9(b) shows the corresponding plot for the elliptical planform airfoil. The time instant for these plots corresponds to that of Figure 7(d), ie. when the foil is at the lower extreme of its heave cycle. The key features observed in both these plots are the vortex loops and ring-like structures which seem to dominate the wakes of these low aspect ratio flapping foils. It should be noted that Drucker & Lauder [17] have observed the formation of vortex rings from the low-aspect ratio pectoral fin of a Bluegill sunfish. It is also interesting to note that these vortex structures are reminiscent of those found in axisymmetric wakes [20] and therefore the correspondence between the wake topologies of drag and thrust producing *cylinders* extends to three-dimensional bodies also. However, the similarity between 2D and 3D flapping foil wakes seems to end there. The dynamics of vortex loops tend to be dominated by the streamwise oriented "legs" of the loops which can be modified significantly due to the shear in the wake. Furthermore, these legs also contribute significantly to the streamwise momentum in the wake and are consequently a key determining factor for the thrust of the flapping foil.

The diminished importance of spanwise vorticity in the wake of low-aspect ratio flapping foil is best seen by examining the spanwise vorticity plot on the foil mid-span which

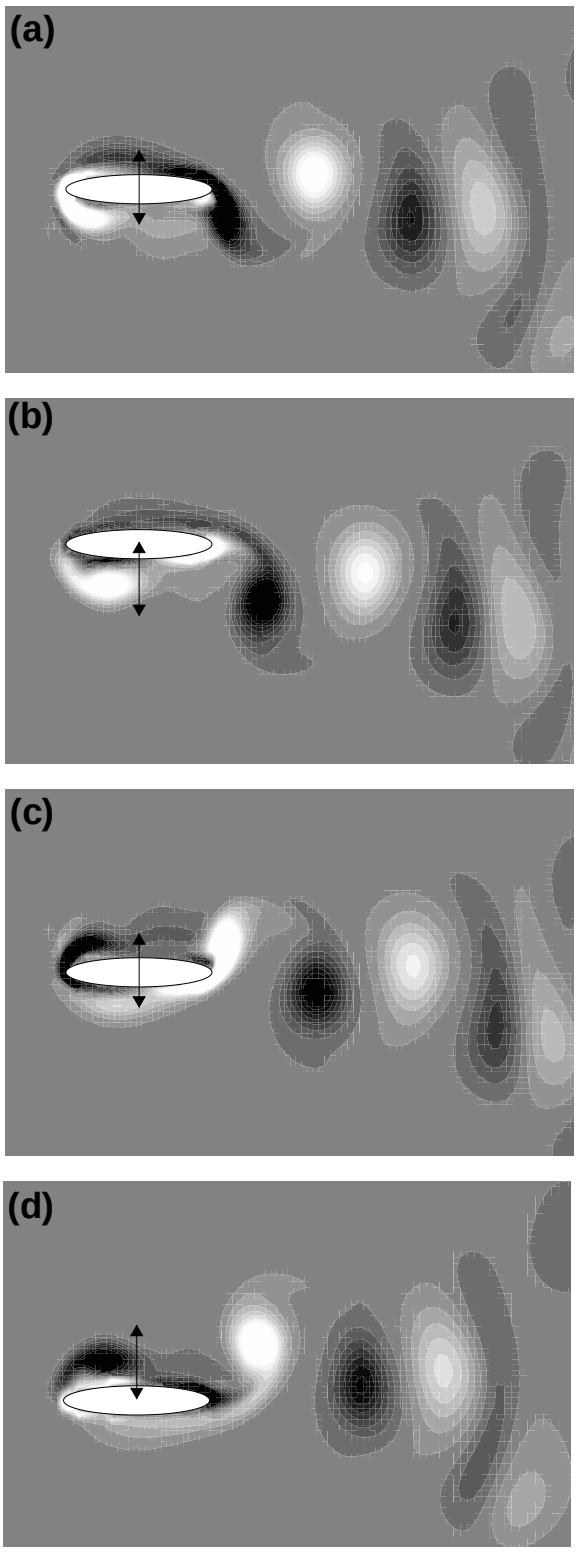

Fig. 7. Spanwise vorticity contour plots for a 2D heaving foil at four different phases in the cycle. (a) $\omega t = 0$ (b) $\pi/2$ (c) π (d) $3\pi/2$

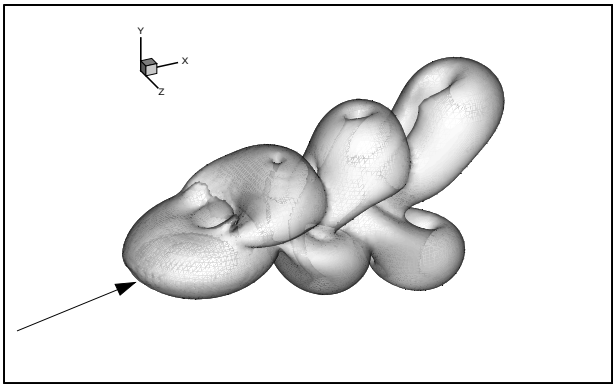

Fig. 8. Enstrophy isosurface plot for the circular disk heaving foil at phase $\omega t = 3\pi/2$. The arrow indicates the direction of the freestream.

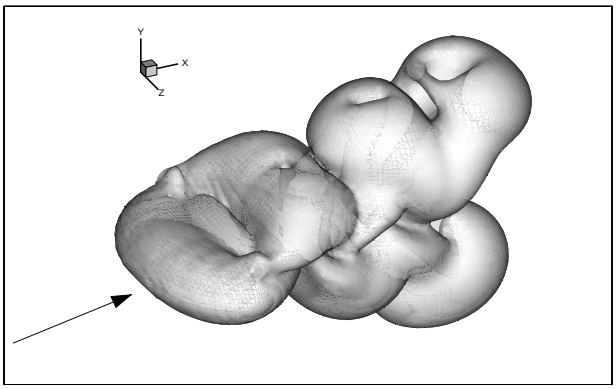

Fig. 9. Enstrophy isosurface plot for the elliptical planform disk heaving foil at phase $\omega t = 3\pi/2$.

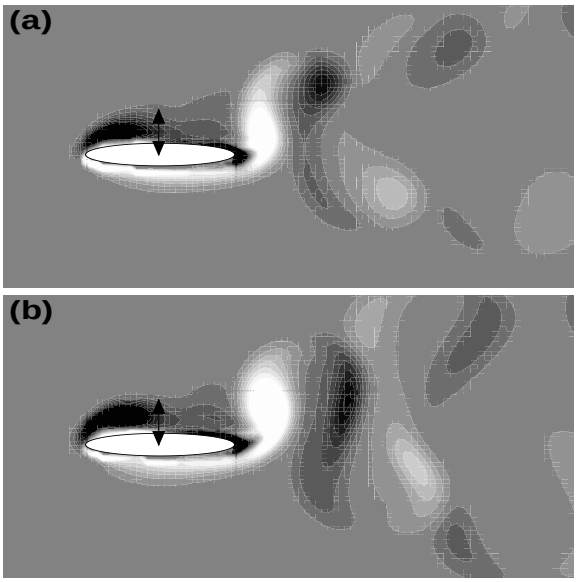

Fig. 10. Spanwise vorticity contour plot at foil mid-span for low-aspect ratio foils. (a) circular disk (b) elliptical planform. foil.

is shown in Figure 10 for the circular disk and elliptical planform foils. The phase for these two plots corresponds to the enstrophy plots in the previous two figures and can be compared directly with Figure 7(d) for the 2D flapping foil. The concentrated spanwise vorticity seen in these plots corresponds to the "heads" of the vortex loops and these are found to be of a relatively lower strength and spaced farther apart from each other than the 2D flapping foil case. Consequently, it is expected that the spanwise vorticity will have a relatively minor contribution to the streamwise momentum balance in the wake. An extensive computational analysis of these low aspect-ratio flapping foils is currently being conducted and results from this study will be presented in the future.

V. Conclusion

A new finite-difference based Cartesian grid method has been developed which allows us to simulate flows with complex 3-D moving bodies. The method has been used to simulate and examine the flow associated with 2D and 3D flapping foils. A study of a 2D flapping foil with an imposed pitch-bias indicates that this control parameter could be effective in producing forces and moments required for rapid pitching and rolling maneuvers. A sequence of simulations have been performed in order to examine the effect of foil aspect-ratio on their performance and wake topology. Simulations indicate that low aspect-ratio foils produce wakes that are significantly different from their 2D counterparts and further analysis is needed in order to gain better insight into these issues.

Acknowledgment

This work is supported under ONR Grant N000140310458 monitored by Dr. P. Bandyopadhyay.

References

[1] F. E. Fish, G. V. Lauder, R. Mittal, A. H. Techet, M. S. Triantafyllou, J. A. Walker, and P. W. Webb, *Conceptual Design for the Construction of a Biorobotic AUV Based on Biological Hydrodynamics*, Proceedings of 13th International Symposium on Unmanned Untethered Submersible Technology (UUST), Durham, New Hampshire, USA August 2003.

[2] C.P. Ellington, *The aerodynamics of hovering insect flight. IV Aerodynamic mechanisms*, Phil. Trans. Roy. Soc. Lon. Ser. B, 305, 79-113, 1984.

[3] M. H. Dickinson, F. O. Lehmann, and S. P. Sane, *Wing Rotation and the Aerodynamic Basics of Insect Flight*, Science 284:1954-1960, 1999.

[4] M. M. Koochesfahani. *Vortical Patterns in the Wake of an Oscillating Airfoil*, AIAA 87-0111, AIAA 25th Aerospace Sciences Meeting, Reno, NV, Jan. 12-15, 1987.

[5] G. S. Triantafyllou, M. S. Triantafyllou and M. A. Grosenbaugh, *Optimal thrust development in oscillating foils with applications to fish propulsion*. J. Fluids Struc. 7, 205-224, 1992.

[6] J. M. Anderson, K. Streitlien, D. S. Barrett and M. S. Triantafyllou, *Oscillating Foils of High Propulsive Efficiency*, J. Fluid Mech. 360:41-72, 1998.

[7] R. Löhner, J.D. Baum, E.L. Mestreau, D. Sharov, Ch. Charman and D. Pelessone - Adaptive Embedded Unstructured Grid Methods; AIAA-03-1116, 2003.

[8] R. Ramamurti, W. C. Sandberg, R. Lhner, J. A. Walker and M. W. Westneat, *Fluid dynamics of flapping aquatic flight in the bird wrasse: 3-D unsteady computations with fin deformation*, Journal of Experimental Biology, 205:2997-3008, 2002.

[9] T. Ye, R. Mittal, H. S. Udaykumar, and W. Shyy, *An accurate Cartesian grid method for simulation of viscous incompressible flows with complex immersed boundaries*. J. Comput. Phys., 156, 209-240, 1999.

[10] H.S. Udaykumar, R. Mittal, P. Rampunggoon and A. Khanna. *A Sharp Interface Cartesian Grid Method for Simulating Flows with Complex Moving Boundaries*, J. Comput. Phys. 174, 345-380, 2001.

[11] R. Mittal, Y. Utturkar and H. S. Udaykumar, *Computational modeling and analysis of biomimetic flight mechanisms*, AIAA 2002-0865. 40th Aerospace Sciences Meeting and Exhibit, Reno, NV. January 2002.

[12] R. Mittal, P. Rampunggoon, *On the virtual aero shaping effect of synthethic jets*, Phys. Fluids, Vol 14, No 4, 2002.

[13] C.H.K. Williamson, *Vortex Dynamics in the Cylinder Wake*, Ann. Rev. Fluid Mech., 28, pp. 477, 1996.

[14] M. Braza, P. Chassiang, and H. Ha Minh, *Numerical Study and Physical Analysis of the Pressure and Velocity Fields in the Near Wake of a Circular Cylinder*, J. Fluid Mech., 165, pp. 79, 1986.

[15] M.S. Triantafyllou, F.S. Hover, S. Licht *The Mechanics Of Force Production In Flapping Foils Under Steady-State And Transient Motion Conditions*, MIT Department of Ocean Engineering, Testing Tank Facility Report 031903, 2003.

[16] J. R. Hove, L. M. O'Bryan, M. S. Gordon, P. W. Webb, and D. Weihs, *Boxfishes (Teleostie: Ostraciidae) as a model system for fishes swimming with many fins: I. Kinematics*, J. Exp. Biol. 204: 1459-1471, 2001.

[17] E. Drucker and G. Lauder, *Experimental hydrodynamics of fish locomotion: functional insights from wake visualization*, Integ. and Comp. Biol. 42:243-257, 2002.

[18] R. Ramamurti and W. C. Sandberg, *A Three-Dimensional Computational Study of the Aerodynamic Mechanisms of Insect Flight*, J. Exp. Biol., Vol. 205, No. 10, pp. 1507-1518, 2002.

[19] H. Liu, C.P. Ellington, K. Kawachi, C. van den Berg, A.P. Willmott, *A Computational Fluid Dynamic Study of Hawkmoth Hovering*, J. Exp. Bio., 201(4), 461-477, 1998.

[20] R. Mittal, J. J. Wilson, F. M. Najjar, *Symmetry properties of the transitional sphere wake*, AIAA J., Vol. 40, No 3, 2002.